

## Article

# Equivalent Impedance Calculation Method for Control Stability Assessment in HVDC Grids

Fisnik Loku <sup>1,\*</sup> , Patrick Düllmann <sup>1</sup> , Christina Brantl <sup>1</sup> and Antonello Monti <sup>2</sup>

<sup>1</sup> Institute of High Voltage Equipment and Grids, Digitalization and Energy Economics, RWTH Aachen University, Templergraben 55, 52062 Aachen, Germany; p.duellmann@iaew.rwth-aachen.de (P.D.); c.brantl@iaew.rwth-aachen.de (C.B.)

<sup>2</sup> E.ON Energy Research Center, Institute for Automation of Complex Power Systems, RWTH Aachen University, Mathieustraße 10, 52074 Aachen, Germany; amonti@eonerc.rwth-aachen.de

\* Correspondence: fisnik.loku@rwth-aachen.de; Tel.: +49-241-8094944

**Abstract:** A major challenge in the development of multi-vendor HVDC networks are converter control interactions. While recent publications have reported interoperability issues such as persistent oscillations for first multi-vendor HVDC setups with AC-side coupling, multi-terminal HVDC networks are expected to face similar challenges. To investigate DC-side control interactions and mitigate possible interoperability issues, several methods based on the converters' and DC network's impedances have been proposed in literature. For DC network's impedance modelling, most methods require detailed knowledge of all converters' design and controls. However, in multi-vendor HVDC networks, converter control parameters are not expected to be shared due to proprietary reasons. Therefore, to facilitate impedance-based stability analyses in multi-vendor MTDC networks, methods that do not require the disclosure of the existing converter controls are needed. Here, detailed impedance measurements can be applied; however, they are time-consuming and require new measurement for a single configuration change. This paper proposes an equivalent impedance calculation method suitable for multi-vendor DC networks, which for available black-box models or converter impedance characteristics can be modularly applied for various network configurations, including different control settings and operating points, while significantly reducing the required time for obtaining an equivalent DC network impedance.

**Keywords:** converter-driven stability; MTDC Interoperability; multi-vendor MTDC networks; impedance calculation



**Citation:** Loku, F.; Düllmann, P.; Brantl, C.; Monti, A. Equivalent Impedance Calculation Method for Control Stability Assessment in HVDC Grids. *Energies* **2021**, *14*, 6899. <https://doi.org/10.3390/en14216899>

Academic Editor: Mario Marchesoni

Received: 10 September 2021

Accepted: 19 October 2021

Published: 21 October 2021

**Publisher's Note:** MDPI stays neutral with regard to jurisdictional claims in published maps and institutional affiliations.



**Copyright:** © 2021 by the authors. Licensee MDPI, Basel, Switzerland. This article is an open access article distributed under the terms and conditions of the Creative Commons Attribution (CC BY) license (<https://creativecommons.org/licenses/by/4.0/>).

## 1. Introduction

State-of-the-art point-to-point HVDC links, mainly utilized for the integration of renewable energy sources and as interconnectors between asynchronous AC transmission systems, are envisaged to develop into multi-terminal DC (MTDC) networks to increase the operational flexibility and the reliability in case of faults, and thus provide a secure power supply [1–3]. However, prior to the implementation of MTDC networks, several key technological challenges must be addressed, such as possible control interoperability issues that may lead to instabilities and as a consequence to undesired emergency shutdowns of the entire MTDC system, jeopardizing the aforementioned purpose of connecting multiple DC links. Several control interoperability issues have been observed in real systems containing multiple power electronic converters, such as oscillations of 2.5 Hz and 97.5 Hz between static synchronous compensators and weak AC/DC grids in the China Southern Grid, or between wind turbines and weak AC grids in Xinjiang, China [4]. To account for these new phenomena, the traditional stability classifications have been extended to include converter-driven stability. The newly added classifications are Slow- and Fast-Interaction converter-driven stability [4]. Generally, control interaction or interoperability issues can arise during various situations, such as steady-state operation, load-flow change,

disconnection or connection of converter stations, faults, or during certain protection actions [5]. Although these interoperability issues have been mainly observed for AC-side coupled converters, similar interoperability issues can be expected for multi-vendor MTDC applications, as investigated in the Best Paths project [5]. Therefore, new methods to ensure stability for these newly defined interactions are needed for future MTDC systems. To this end several publications propose a stability analysis based on an analytical analysis of linear models of state-of-the-art Modular Multilevel Converters (MMCs) and their controls [6,7], or entire MTDC systems including detailed DC-side impedance models of MMCs with the complete converter control [8]. While these works significantly contribute to stability analysis in MTDC networks, a major disadvantage of these white-box approaches is that they require detailed knowledge about the structure of the MMC control systems. Therefore, they are not applicable for multi-vendor based MTDC networks, as the disclosure and exchange of sufficiently accurate analytical converter and control models is highly improbable due to proprietary reasons [5,9]. Instead of using a single whitebox model for stability assessment of a DC network, a modular approach with defined interfaces could be used. A suitable and widely applied method for system stability analysis is the impedance-based stability criterion, which states that any system can be separated as a Thevenin or a Norton equivalent circuit, as shown in Figure 1. The stability of the overall system can then be analyzed by considering the ratio of the corresponding impedances of both equivalent circuits and applying the Nyquist stability criterion [10]. In the case of a multi-vendor HVDC systems, a split into  $Z_{MMC}$  and  $Z_{grid}$  can be considered. Depending on the available information, both  $Z_{MMC}$  and  $Z_{grid}$  could be calculated using a frequency sweep approach or provided by either the respective grid operator or converter manufacturer, so that stability analyses can be conducted without the need for converter-internal data. Whereas previous literature mainly focuses on the derivation of the MMCs' equivalent impedance  $Z_{MMC}$ —either in an analytical way [6–8] or via using frequency sweep measurements [11,12]—the DC network and the corresponding  $Z_{grid}$  are often modeled in a simplified way; for example, DC cables are assumed as simple Pi-section models, which are very limited with regard to modeling the frequency dependent impedance behavior [13]. Hence, the overall DC grid impedance  $Z_{grid}$  relevant for stability analyses can only be derived for a small bandwidth of lower frequencies. Because of this limitation, in most previous studies no further investigation regarding the impact of possible DC network topologies on the system stability is considered.

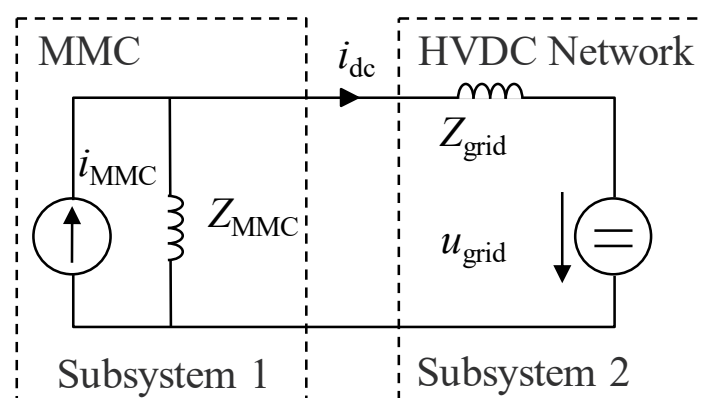


**Figure 1.** Impedance based stability criterion.

However, HVDC networks can have different topologies such as point-to-point, radial, or meshed, where several combinations regarding network design and cable lengths are possible, resulting in a multitude of prospective grid impedances  $Z_{grid}$ . Therefore, a detailed model of the network is critical for MTDC networks, and one of the key elements is the frequency dependency of the cable model. Furthermore, the network impedance seen from the DC terminal of a converter also depends on the control modes and operating points of all the other converters in the system, resulting in numerous factors influencing

the impedance  $Z_{\text{grid}}$  with which a converter is prospectively interacting. Due to the resulting complexity, there is no method yet to identify critical cases in advance, thus a large number of combinations has to be analyzed to assess and ensure system stability. Therefore, the other key element is the equivalent impedance of the converters. To obtain the equivalent impedance of an HVDC network ( $Z_{\text{grid}}$ ) consisting of black-boxed MMC models and detailed frequency dependent cable models, simulative frequency sweep methods can be applied to properly capture the frequency dependency. However, using this simulative approach would require a new measurement for each network or MMC control modification, which is a time-consuming process. Alternative methods are needed that enable faster and adaptable analyses with the aim to identify critical cases.

In this paper, a modular analytical approach to derive the equivalent network impedance applicable for stability analyses in multi-vendor based MTDC networks is proposed that (a) allows for the use of black-boxed MMC models, (b) is capable to calculate all possible DC network impedances in a short time with sufficient accuracy, and (c) enables an analysis of different combinations of network topologies, operating points, and control modes. The method relies on the availability of the MMC and DC cable impedances. Provided that the DC-side impedance behavior of the MMCs is given for several control modes and operating points, no further details of converters are required to accurately calculate the equivalent impedance behavior of a DC grid as seen from the DC terminals of any MMC of interest. These impedances can be obtained from the vendors or by using an appropriate frequency sweep method (as applied in this paper). The impedance of the cables could either be given by the respective system operator or derived thanks to the availability of the cable data. To accurately represent the DC cables for the impedance-based analysis, frequency dependent (FD) Pi-sections as proposed in [13,14] are needed. This way, a DC network's cables can be accurately represented up to an upper frequency limit of several kHz, covering the aforementioned bandwidth relevant to assess fast-interaction phenomena. The frequency range of up to 1 kHz is the focus of this paper, as it incorporates Fast-Interaction converter-driven stability range, that is defined to be in several hundred of Hz and possibly reach kHz [4]. Given these appropriately derived impedances, the proposed method allows a fast impedance-based analysis for a multitude of possible system topologies, control modes, and operating points, such that HVDC network stability can be investigated comprehensively and impact factors and worst-case operating scenarios can be derived, allowing the application of methods to enhance the interoperability and stability.

The paper is organized as follows: As a basis, the MMC converter design and relevant control structures are introduced in Sections 2.1 and 2.2, respectively. Furthermore, appropriate modeling of the DC cables as a frequency-dependent model and FD Pi sections is presented in Section 2.3. In Section 3, it is explained how the DC network impedance seen from a specific MMC can be obtained. In Section 3.1, the simulation-based measurement method used for verification is explained, before the analytical method proposed in this paper is introduced in Section 3.2. Moreover, in Section 4, a procedure to obtain the MMCs' impedance charts required for the application of the proposed method is described. In Section 4.1, the influence of the MMC control modes and different operating points is analyzed, which are required for the validation of the proposed method. In Section 5.1, the proposed method is validated for a radial and a meshed MTDC network, where the calculated network impedances are compared to corresponding measured impedances. To assess its applicability, the proposed network estimation method is applied for an impedance-based stability analysis of a MTDC network in Section 5.2.

## 2. MMC and Cable Representation for Impedance-Based Analysis

In this section, the design of the MMCs, their controls, and the modeling of the DC cables are described as building blocks that are required for the development of the equivalent impedance calculation method proposed in this paper.

### 2.1. MMC Design

Since no impedance models of a black-boxed MMC from a specific vendor are available for the investigations in this paper, the MMC stations are simulated as Type 4 average models. They are adequate for the control interoperability studies and are used to obtain the example frequency-dependent impedance data [15]. A schematic representation of an MMC is shown in Figure 2 [16]. The parameters of the converter stations used in this paper are summarized in Table 1. On the AC side, the AC grids are modeled as Thevenin equivalents with a rated apparent power  $S_{nom} = 30$  GVA and at a rated phase-to-phase AC voltage of  $u_{AC,1} = 400$  kV with a nominal frequency of  $f_{nom} = 50$  Hz. The calculations, and corresponding simulations, are done with MATLAB/SIMULINK with a time step of  $\Delta t_{sim} = 40 \mu s$ .

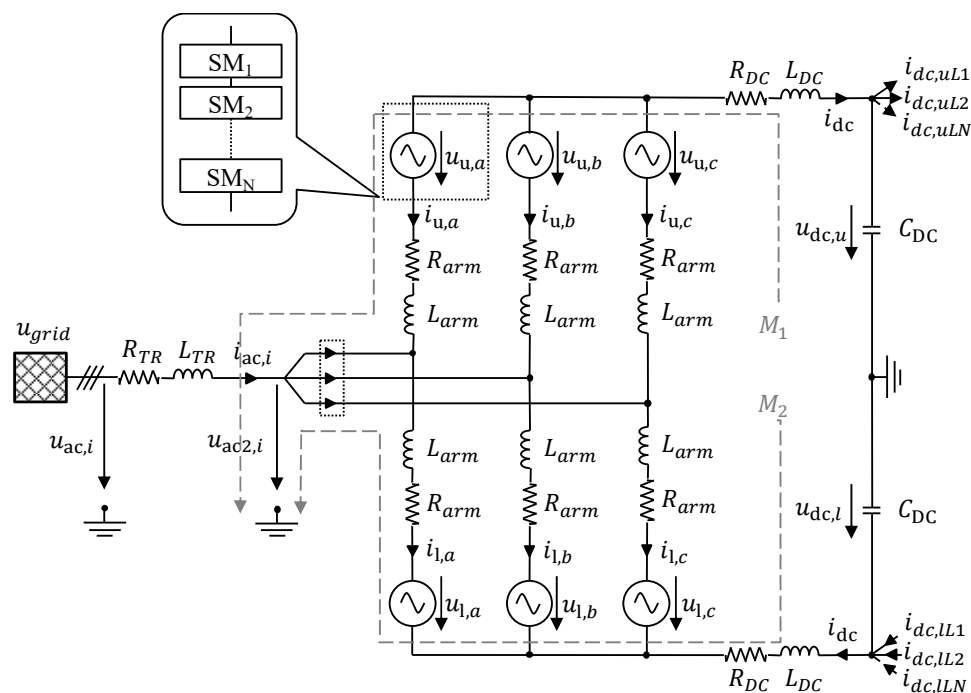


Figure 2. Schematic representation of an MMC.

Table 1. MMC Parameters.

MMC Parameter	Abbr.	Value
Nominal DC voltage	$u_{DC,n}$	$\pm 320$ kV
Nominal DC current	$i_{DC,n}$	1.875 kA
Nominal output power	$P_{DC,n}$	1200 MW
Nominal AC voltage	$u_{AC,1}$	400 kV
LL-RMS	$u_{AC,2}$	350 kV

### 2.2. MMC Controls

Considering that this paper focuses on impedance calculation suitable for black-box models, any MMC control can be applied, i.e., non-energy or energy-based MMC controls. The exemplary MMC controls used for the investigations in this paper are energy-based controls with the cascaded vector control structure shown in Figure 3 [16].

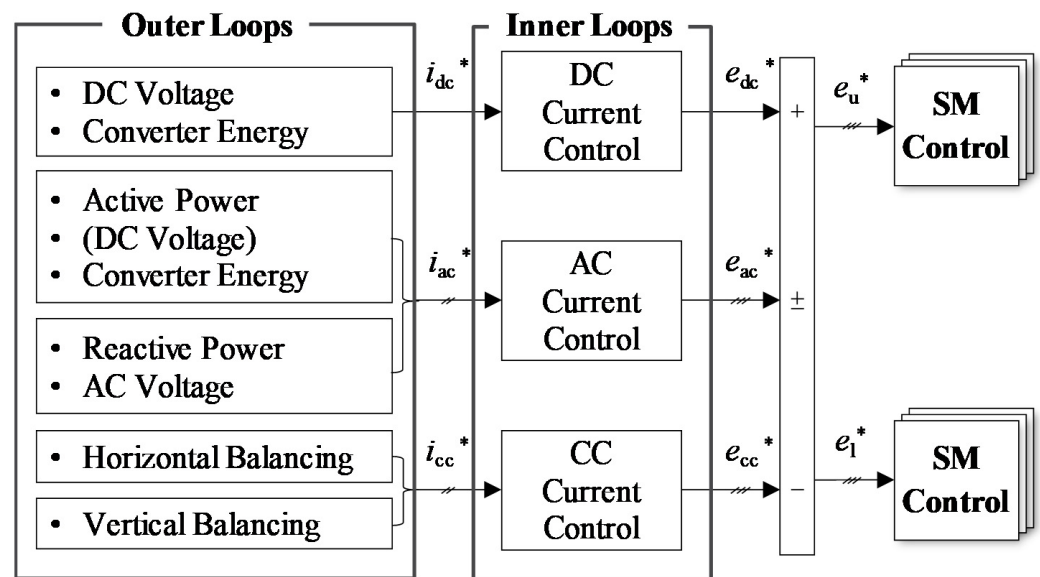


Figure 3. MMC Control Structure (reference signals denoted with (\*)).

The outer loop control provides the reference values to the inner loops, which comprise the AC current control, DC current control, and the circulating current (CC) controls. The inner loops then provide the reference values for the calculation of the reference phase-arm voltages of the MMC. The DC voltage control, DC current control, and the total energy balancing control are assumed to have the highest impact on the DC side impedance of the converters [17]. To systematically compare the influence of control parameters on the MMCs' impedance, the symmetrical optimum (SO) method, where a control loop phase-margin  $\varphi_M$  can be pre-defined, is exemplarily applied here for both DC voltage and TEB control loops [16]. For the standard SO, the value of the phase-margin is  $\varphi_M 36.9^\circ$ . For a generalized SO, a phase-margin in the range of  $36.9^\circ \leq \varphi_M \leq 61.9^\circ$  is recommended. A higher value of  $\varphi_M$  leads to an improved damping but a slower system response [18,19].

### 2.3. DC Cables

For the time-domain simulations used for validation (cf. Section 5), the DC cables are modeled using a frequency-dependent universal line model (ULM) developed within BEST PATHS [20]. The cable parameters required for the model are extracted from a 320-kV XLPE submarine cable design in PSCAD/EMTDC. The parameters of the DC cable are copper core conductors with resistivity of  $\rho = 1.72 \times 10^{-8}$  [ $\Omega\text{m}$ ] of cross sections of  $A_{\text{core}} = 1984 \text{ mm}^2$  based on a benchmark case in [15]. While the frequency-dependent cable models, such as the ULM, represent the DC cable behavior very accurately, combining them with the impedance behavior of the MMCs to analytically calculate the equivalent DC network impedance is not applicable. Due to the two-port network nature, they are not suited for analytical calculations, but only for corresponding simulations [13]. To address this issue, ULMs can generally be represented by simple Pi-sections, consisting of a single RL branch or frequency dependent (FD) Pi-sections, consisting of cascaded Pi-sections with several parallel RL branches. A configuration of a FD Pi-section is shown in Figure 4. Here, the elements of the Pi-sections are calculated as proposed by [13,14].

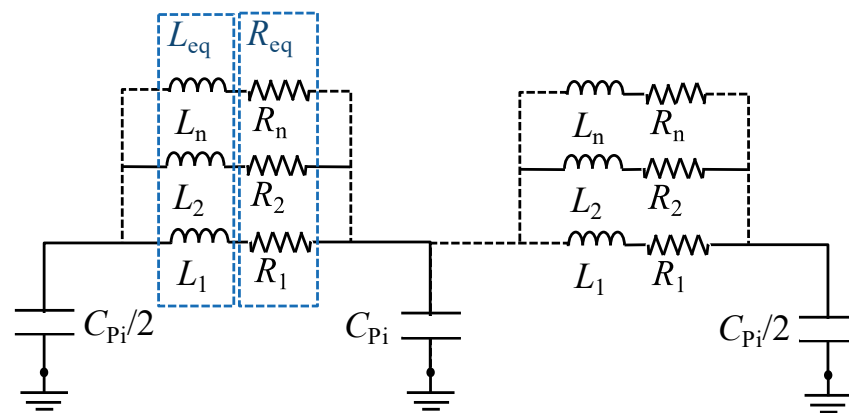


Figure 4. FD-Pi sections.

Considering that a higher number of the cascaded Pi-sections and parallel branches results in transfer functions of a higher order, a configuration of four cascaded Pi-sections with three parallel branches each is considered in this paper. This configuration shows a very good approximation of the DC cable impedance behavior for frequencies up to  $f = 1$  kHz [13]. The corresponding per single Pi-section unit length values of a simple Pi-section and FD Pi-sections corresponding to the DC cable design are shown in Table 2.

Table 2. Equivalent simple and FD-Pi Section values.

Pi-Section Element	Simple Pi-Section		FD Pi-Section	
		Branch 1	Branch 2	Branch 3
Resistance [Ohm/km]	$8.67 \times 10^{-3}$	$1.54/n_{Pi}$	$8.77 \times 10^{-2}/n_{Pi}$	$9.68 \times 10^{-3}/n_{Pi}$
Inductance [H/km]	$3.01 \times 10^{-5}$	$3.02 \times 10^{-5}/n_{Pi}$	$2.74 \times 10^{-4}/n_{Pi}$	$2.65 \times 10^{-3}/n_{Pi}$
Capacitance [F/km]	$2.76 \times 10^{-7}$		$2.76 \times 10^{-7}/n_{Pi}$	

### 3. DC-Network Impedance Derivation Methods

In this section, a simulative approach for the equivalent impedance measurement of a DC network as seen from the terminals of an involved MMC using a frequency sweep method is initially explained in Section 3.1. The frequency sweep approach is adapted from existing frequency sweep approaches for the AC side impedance derivations. Then, the proposed approach to calculate this equivalent impedance from the single elements of the network is presented in Section 3.2.

#### 3.1. DC Network Impedance Measurement

The equivalent DC network impedance is measured by applying a frequency-sweep-based method to the implemented Simulink model. The used method is adapted from AC-side impedance measurements of the MMCs and is also suitable for cases in which the MMCs are only available as black-boxes [11,21]. Depending on the control mode (DC voltage or active power) of the MMCs from which the equivalent impedance of the DC network is measured, a DC voltage source at the DC voltage nominal value, or a current source at the corresponding operating point is connected to the DC terminals of the corresponding MMCs, respectively. A perturbation voltage or current is added in series on the positive pole with the respective source, to obtain an equivalent impedance between the positive and the negative pole, (see Figure 5a). The perturbation magnitude is set to 1% of the corresponding nominal value, such that any unwanted control reactions of the connected MMCs are avoided. For each perturbation frequency, the DC network impedance results as the ratio of the measured voltage and current. The amplitude and phase of the obtained impedance points are calculated by applying Fourier analysis. This way, the equivalent impedance of the DC network as seen from the DC terminal of an MMC can be obtained for the different control modes and different operating points of the MMCs

in the DC network. While this simulation-based DC network impedance measurement method can be used to obtain the impedance behavior as an input to impedance-based stability analyses for various DC network configurations at different MMC operating points, it is very time-consuming. To address this issue, an equivalent DC network impedance calculation approach is proposed in the next Section.

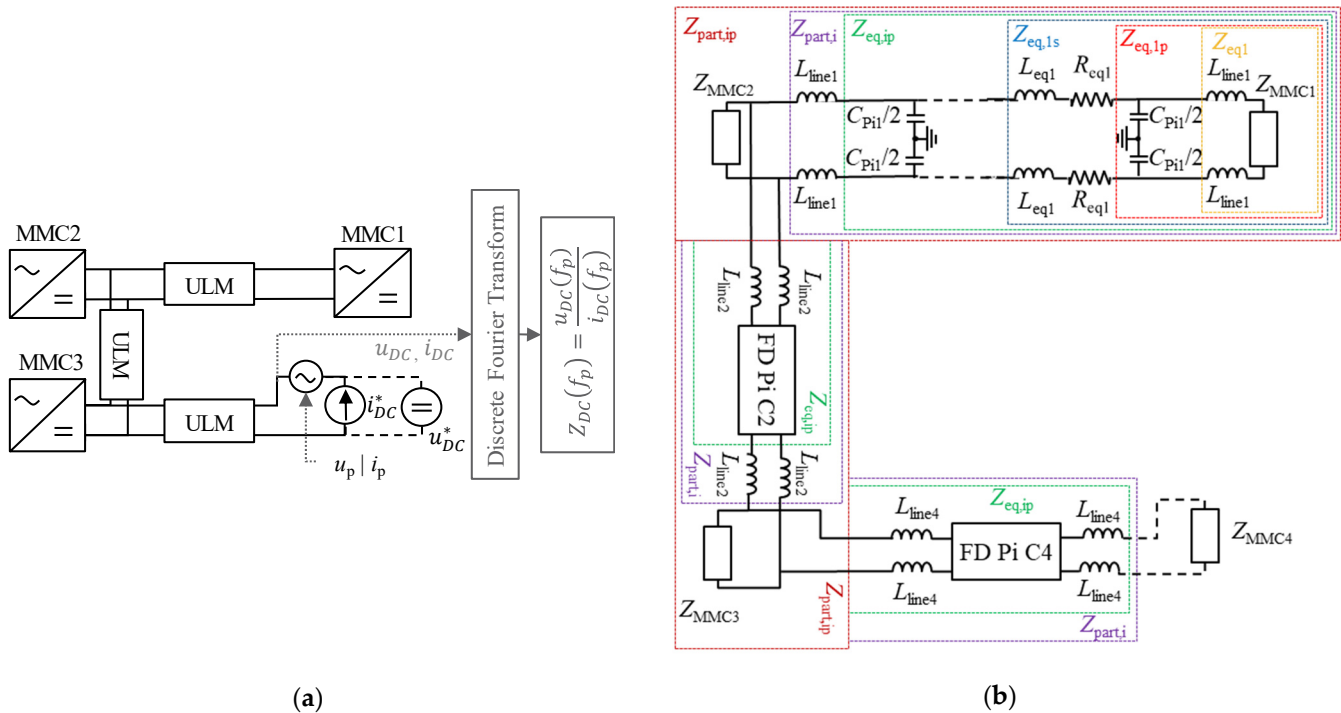


Figure 5. Equivalent impedance measurement (a) and calculation method (b), e.g., as seen from MMC 4.

### 3.2. Proposed Methodology to Calculate the Equivalent Impedance of a MTDC Network

For an equivalent DC network impedance calculation, as seen from any MMC within the network, the impedance of the DC cables needs to be properly combined with the impedance of the other MMCs. Provided that the equivalent impedance of all MMCs in an existing DC network are given, the DC network equivalent impedance as seen from an MMC can be calculated analytically by an iterative process, via the following steps:

1. Each MMC impedance  $Z_{MMC}$  is regarded as a single impedance between the positive and negative DC terminals. It can be measured as explained in Section 4, or be provided by the corresponding manufacturer. Furthermore, future MTDC systems are expected to feature DCCB based protection, which require line inductors at each line end to limit the rate of rise of current [15]. To consider their influence on the dynamic system behavior, example DC line inductors  $L_{line}$  are considered here.
2. Define the MMC (reference MMC) and thereby point of connection at which the DC network impedance should be calculated. The equivalent network impedance as seen from the DC terminals of the reference MMC is calculated by starting from the DC cable end that has only a single connection to an equivalent impedance, e.g., MMC 1 in Figure 5b). This MMC's impedance is connected in series with the corresponding DC line inductors  $L_{line}$ , such that  $Z_{eq,i} = Z_{MMC,i} + 2 \cdot Z_{L,line,i}$ .
3. The positive and negative pole DC cables are represented via (FD) Pi-sections, as derived in Section 2.3, whose capacitances are considered in series for the steady-state case. The equivalent impedance  $Z_{eq,i}$  from step 2 is in parallel with the capacitances of the Pi-sections, which results in  $Z_{eq,ip} = 1 / ((1 / Z_{eq,i}) + 0.5 \cdot (1 / Z_{C_{Pi}/2}))$ .

4. The series impedances of (FD) Pi-sections  $Z_{b,eq}$  are added in series to  $Z_{eq,ip}$  resulting in  $Z_{eq,is} = Z_{eq,ip} + 2 \cdot Z_{b,eq}$ . Steps 3–4 are repeated until the end of the (FD) Pi-sections for the corresponding radial connection is reached.
5. After step 4, the  $L_{line}$  at the end of the corresponding (FD) Pi-sections are added in series to obtain a partial network impedance  $Z_{part,i} = Z_{eq,ip} + 2 \cdot Z_{L,line}$  as seen from the point of common coupling (PCC).
6. In case of another radial connection at PCC  $Z_{part,ij}$  that does not include the reference MMC, steps 1–5 are applied to derive  $Z_{part,ij}$  is in parallel to  $Z_{part,i}$  from step 5, resulting in  $Z_{part,ip} = 1 / ((1/Z_{part,i}) + (1/Z_{part,ij}))$ .  $Z_{part,ij}$  can also be an MMC equivalent impedance, in which case  $Z_{part,ij}$  would be replaced by a corresponding  $Z_{MMC,ij}$ .

Each step involves equivalent impedances represented as higher-order transfer functions (TFs). In order to avoid computational overflow in the multiple calculation steps, after each step a reduction of the TFs is applied while conserving the dynamics of the calculated equivalent impedance. Regarding a meshed network configuration, steps 1–6 would ideally be applied after a  $\Delta/Y$  transformation of the corresponding ring network which would result in parallel connected radial network parts. However, a  $\Delta/Y$  transformation of the DC cables here is not applicable as they would need to be considered separately from the corresponding MMC/network-part impedances, thus leading to the same reasons why ULM cannot be used for the network impedance calculation. Alternatively, MMC/network-part impedances that are connected to the ring network can be assumed to be connected to the reference MMC via two parallel network parts  $Z_{part,ip}$ .

The equivalent impedance measurement of a DC network via simulation (cf. Section 3.1) normally is a time-consuming process, which for an example four-terminal network as shown in Figure 5 takes approximately 5–6 h for one configuration and set-point with Matlab/SIMULINK. The proposed impedance calculation approach takes approximately 1 s. Considering that for each operating point and topology change the equivalent impedances require to be simulated, the proposed approach has an impedance estimation speed advantage over the simulative approach.

As the calculation method requires a corresponding impedance characteristic for each MMC, but no external data is available in this work, a measurement method to obtain the MMCs' impedance for various operating points is presented in Section 4, and corresponding obtained MMC impedance behaviors are analyzed.

#### 4. MMC Impedance Measurement and Analysis

The equivalent DC-side impedance of the MMCs is measured by applying the frequency sweep-based method described in Section 3.1. Similar to the equivalent network impedance measurement, depending on the control mode (DC voltage or active power) of the MMCs, a voltage or a current source is connected to the DC terminals of the MMC station. The sources are set to their corresponding nominal values; a perturbation voltage or current is added in series on the positive terminal of the MMC with the respective source. For complete stability analysis, there are several factors of a DC network that need to be considered, such as the MMC control configurations, load-flow, and different network topologies. Hence, these factors must also be covered within the validation process of the proposed method. As a first step, the MMCs' impedance obtained for various control modes and operating points are presented in Section 4.1.

##### 4.1. Impedance Behavior of the MMCs

In this section, the impedance behavior of the MMCs controlling the DC voltage and the active power are measured for different operating points and control tuning to represent a possible range of MMC impedances. For this, power transfer setpoints of  $P_{ac,ref} = [-1.0, -0.7, -0.5, -0.3, 0, 0.3, 0.5, 0.7, 1.0]$  p.u. are chosen as examples, where the PI control parameters of the outer loops (cf. Section 2.2) are tuned via the standard SO with a PM of  $\varphi_M = 36.9^\circ$ . To observe the influence of the control parameter tuning, MMC impedances for PI control parameters tuned with a PM of  $\varphi_M = 36.9^\circ, 45^\circ, \text{ and } 60^\circ$  for a

fixed load flow scenario are compared. The corresponding lowest and highest PM values are chosen from literature [16,22], while  $\varphi_M = 45^\circ$  is an additional example value used for comparison.

#### 4.1.1. DC Voltage Controlling MMC

In Figure 6 (left), the influence of the operating point on the impedance behavior of the DC voltage controlling MMC is shown.

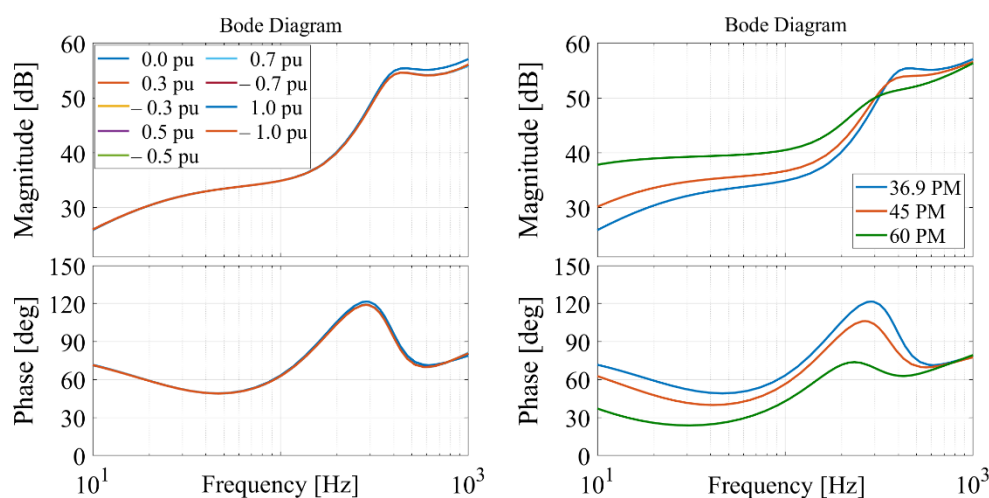


**Figure 6.** DC Voltage Controlling MMC for various working points (left) and different control parameters (right).

It can be seen that for the different operating points, the impedance behavior of the MMC stays approximately the same. This can be explained in two steps: first, the passive impedance of the MMCs is the same irrespective of the controls; second, the active impedance in DC voltage control mode does not depend on the load flow as the MMC manages to control the DC voltage according to the specified PI control parameters, irrespective of the operating point. When different control parameters (i.e., different tuning with  $\varphi_M = 36.9^\circ$ ,  $45^\circ$ , and  $60^\circ$ ) are investigated, a strong influence can be observed: from Figure 6 (right), it can be seen that the amplitude decreases but the phase increases with decreasing PM for low frequencies up to  $f \approx 400$  Hz. For frequencies above 400 Hz, the amplitude of the MMC impedance becomes higher for lower PM of the controls.

#### 4.1.2. Active Power Controlling MMC

The impedance behavior of the active power controlling MMC for the different operating points is shown in Figure 7 (left).

The dependency of the operating point is most significant for frequencies up to  $f \approx 200$  Hz. Here, for higher power transfers from the DC to the AC side of the corresponding MMC, the equivalent MMC impedance has lower magnitude, and the corresponding frequency range where the phase is at  $\sim -180^\circ$  or  $\sim 180^\circ$ , and consequently corresponds to negative damping of the MMC, is larger, the higher the DC to AC power transfer is. The impedance behavior for higher frequencies than 200 Hz can be assumed to be independent of the corresponding operating point. Furthermore, a strong influence of the different control parameters on the MMC impedance can be observed from Figure 7 (right), where for lower control parameters' PM, the magnitude is higher in the frequency range lower than 50 Hz.

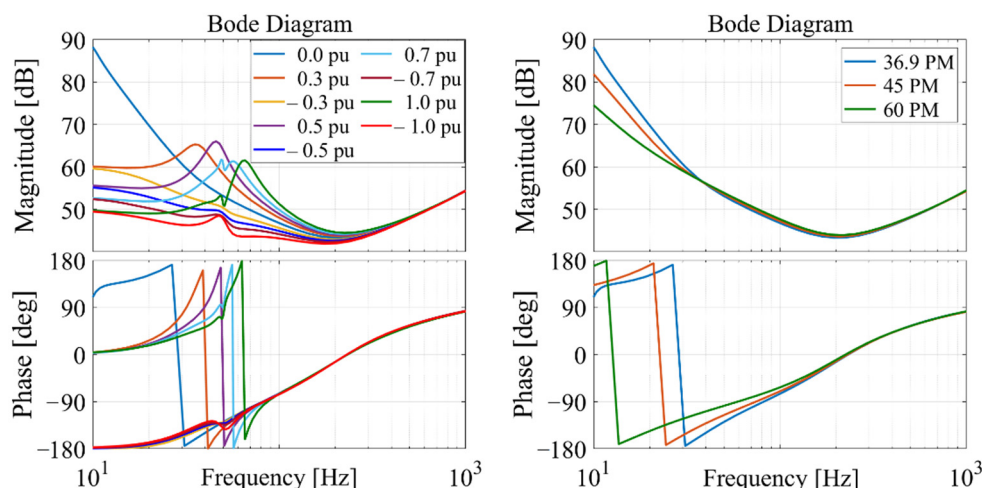


Figure 7. Active power controlling MMC for various working points (left) and different control parameters (right).

### 5. Validation of the Proposed Method and Its Application in an MTDC Network

In Section 5.1, the proposed method is validated for a four-terminal radial and a meshed DC network: The equivalent impedances of the MMCs from Section 4.1 are fed into the method proposed in Section 3.2 to calculate the DC network equivalent impedance as seen from the terminals of each MMC. Lastly, an example application of the proposed method for impedance-based stability analysis is presented in Section 5.2.

#### 5.1. Validation of the Proposed Method

For the validation of the proposed approach for different topologies, both a radial and a meshed setup of the DC network configuration as shown in Figure 8 are evaluated, which consist of MMCs with specifications from Table 1. Furthermore, considering the significant impact of the different control modes and load-flow scenarios on the overall impedance seen from a specific MMC, two cases (case A and B) for different control modes of the MMCs and different load-flows are considered for the radial and meshed networks.

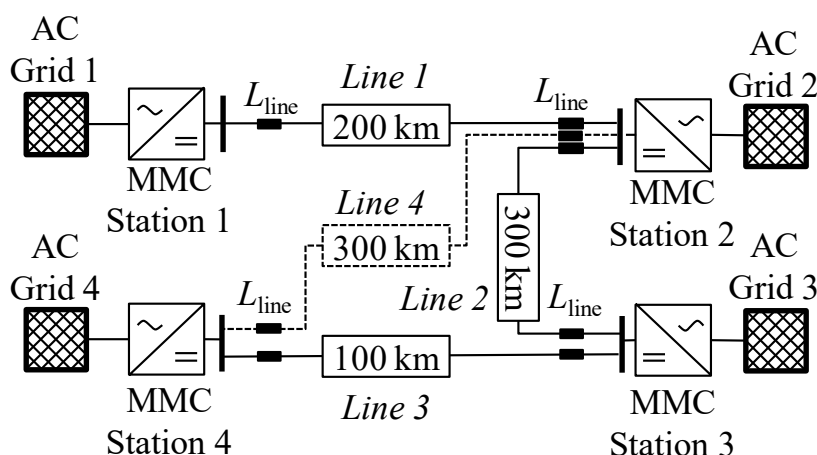
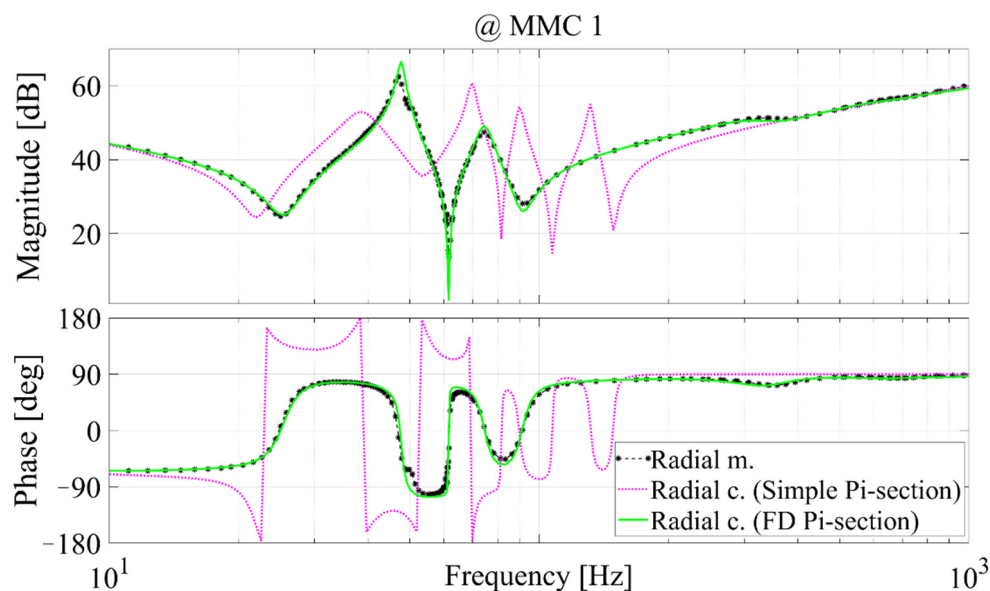


Figure 8. Investigated HVDC system.

For all cases, the inner and the outer loops of the corresponding MMC controls are exemplarily tuned applying the MO, and the standard SO with  $\varphi_M = 36.9^\circ$ . DC line inductors of  $L_{line} = 80$  mH are included at each DC cable end. For both cases, the equivalent impedance of the DC network as seen from each MMC is calculated for both topologies by applying the proposed approach in Section 3.2, and then are compared to the corresponding equivalent impedance measurements in Matlab/SIMULINK, as described in Section 3.1.

For case A, the MMC control modes are chosen such that MMC 1 controls the DC voltage to  $V_{DC,ref} = 1$  p.u. MMC 2, MMC 3, and MMC 4 control the active power to  $P_{ref2} = 0.6$  p.u.,  $P_{ref3} = 0.4$  p.u. and  $P_{ref4} = -0.5$  p.u., respectively. For MMC 1, the same equivalent impedance is used in the calculations as for no load flow, since as shown in Figure 6, the power flow does not influence the equivalent impedance of the DC voltage controlling MMC. In case B, in order to consider different control modes for the validation of the proposed impedance calculation method, MMC 1, MMC 2 and MMC 4 are set to control the active power to  $P_{ref1} = P_{ref2} = 0.5$  p.u. and  $P_{ref4} = 0.0$  p.u., respectively. MMC 3 controls the DC voltage to  $V_{DC,ref} = 1$  p.u.

Considering that both simple Pi-section and FD Pi-section configurations are applied in the literature (cf. Section 1) to represent DC cables, the equivalent network impedance as seen from MMC 1 for case A is initially measured for the radial network comprising frequency-dependent ULMs, and then it is calculated by applying the proposed method in Section 3.2 for the radial network consisting of simple and FD Pi-sections. The comparison results are shown in Figure 9.



**Figure 9.** DC network impedance seen at MMC 1 with simple and FD-Pi sections.

The comparison in Figure 9 shows that the equivalent impedance of the network consisting of simple Pi-sections (magenta, dashed) matches the measured results consisting of ULMs (black with ‘\*’) only for the frequencies lower than  $\sim 15$  Hz. For higher frequencies, significant deviations can be observed. On the other hand, the utilization of FD Pi-sections (green) leads to high matching between the measured and the simulated network impedance as seen from MMC 1. Therefore, FD-Pi sections are used for the further investigations in this section.

The validation results of case A and case B are shown in Figures 10 and 11, respectively. The comparisons from Figures 10 and 11 show that for the radial network the calculated impedances (green) as seen from the different MMCs are almost identical to the corresponding measured impedances (black with ‘\*’). Here, it can be concluded that applying the proposed impedance calculation method results in a highly accurate estimation of different radial network topologies incorporating different MMC control modes and operating points. For the meshed network, differences can be observed between the calculated (red) and the measured (blue with ‘o’) network impedances. Here, for both cases, the calculated impedances of MMC 3 and MMC 4 show amplitude differences to the measured network impedances mainly for the frequency range  $30 \text{ Hz} < f < 60 \text{ Hz}$ . However, for the frequency range up to  $f = 1 \text{ kHz}$ , the calculated network impedance shows similar impedance behavior pattern as the calculated impedance. These differences for the meshed

network are assumed to be due to two main factors: firstly, for complex networks, the errors resulting from the differences between ULM and FD Pi-sections add up. Secondly, in order to avoid computational overflow, a reduction of the resulting higher-order TFs is required (cf. Section 3.2). While the lower-order TF can accurately represent an equivalent impedance of a network part, such as a radial network configuration, errors add up in the calculation process and they become significant when meshed networks are considered, as the corresponding MMC/network-part impedances that are connected to the ring network are assumed to be connected to the reference MMC via more complex network, i.e., two parallel network parts (cf. Section 3.2).

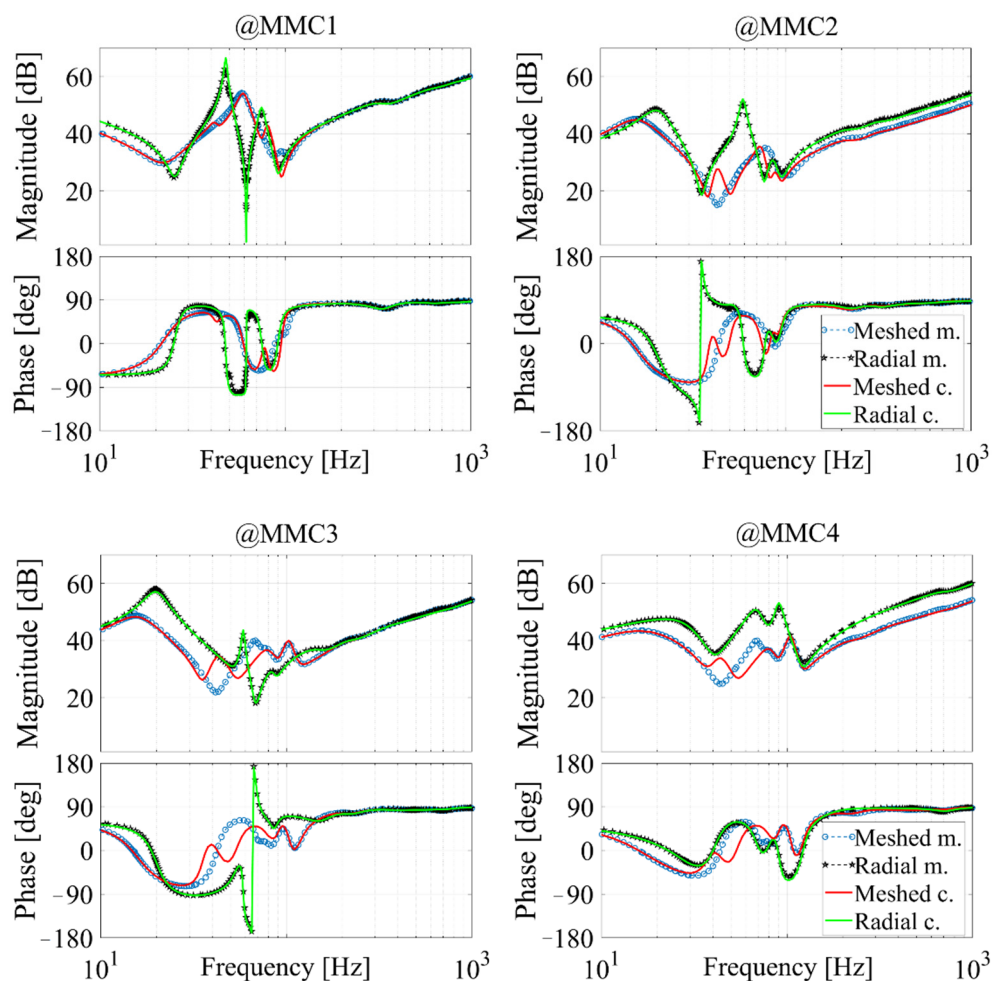


**Figure 10.** Measured vs. calculated radial (black vs. green) and meshed (blue vs. red) network equivalent impedance seen from the four different MMCs.

This assumption is supported when the calculated network impedance as seen from MMC 1 and MMC 2 for both cases is analyzed. In comparison to MMC 3 and MMC 4, which are part of the network's "ring", the difference between the calculated and measured network impedances is smaller for MMC 2, and especially for MMC 1. This is mainly due to the reason that MMC 1 is radially connected to MMC 2 and the equivalent meshed impedance resulting from lines 2, 3, and 4 is in parallel connection to MMC 2, and then radially connected to line 1. Therefore, the impedance of line 1 dominates the overall impedance seen at MMC 1. As the radial connection can be represented with a high accuracy, the errors resulting from the meshed network are accordingly reduced. From the obtained results, it can be concluded that the proposed network impedance calculation method can be utilized for radial networks to achieve a highly accurate network impedance representation. For converters connected to meshed networks, it can be used to obtain

an indication for possible critical interaction points in case of impedance-based stability analysis, which should then be checked by simulations.

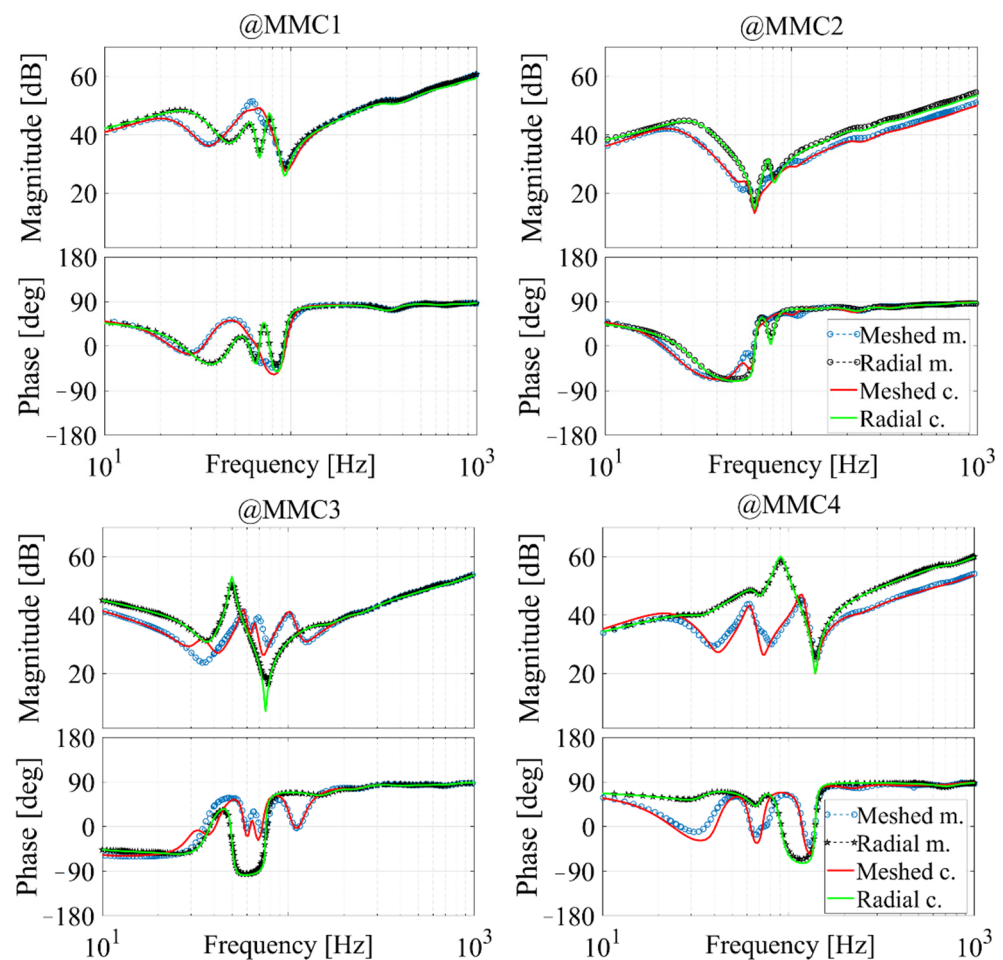


**Figure 11.** Measured vs. calculated radial (black vs. green) and meshed (blue vs. red) network equivalent impedance seen from the four different MMCs.

### 5.2. Example Application to Stability Analysis

To demonstrate the applicability of the proposed impedance calculation approach in Section 3.2 for stability assessment, it is applied to obtain the equivalent impedance of the DC network as seen from the DC terminals of MMC 4 for a large set of possible operating points of the MMCs (The set of operating points refers to only integer reference points here, e.g.  $[-1, -0.9 \dots, 0.9, 1.0]$  p.u.), utilizing the MMC control modes as in case B radial network. The bode diagrams of the obtained equivalent impedances are shown in Figure 12 along with MMC 4 equivalent impedances for all considered operating points, resulting in 331 different cases.

It is worth noting that the impedance calculation with the proposed approach of all cases as seen from a single MMC lasts approx. 5 min, whereas an impedance measurement of a single case lasts at least 5 h. From the impedance-based stability analysis using the bode diagrams in Figure 12 it is determined that regardless of the operating points of the other MMCs, the system becomes unstable if the reference active power for MMC 4 is set to  $P_{\text{ref},4} = -0.6$  p.u. or lower. Therefore, to have a stable DC network as seen from MMC 4, its active power reference must be at least  $P_{\text{ref},4} = -0.5$  p.u. Next, to consider a specific load-flow change, case B is considered, for which the MMC operating points are referred to as operating point OP1. The load-flow is then changed for all active power controlling MMCs, such that  $P_{\text{ref}1} = P_{\text{ref}2} = -0.5$  p.u.,  $P_{\text{ref}4} = 0.7$  p.u., i.e., referred to as operating point OP2. The equivalent DC network impedances as seen from all the MMCs are calculated for

OP2 along with the corresponding MMC impedances at the two different operating points and are shown in Figures 13 and 14.

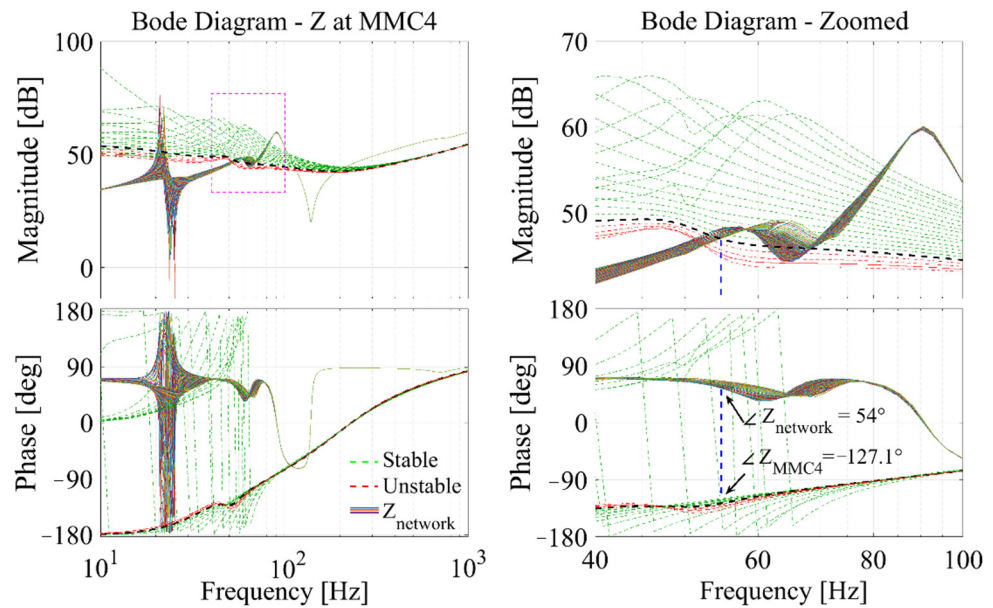


Figure 12. Impedance of MMC station 4 and network impedance seen from the terminals of MMC station 4.

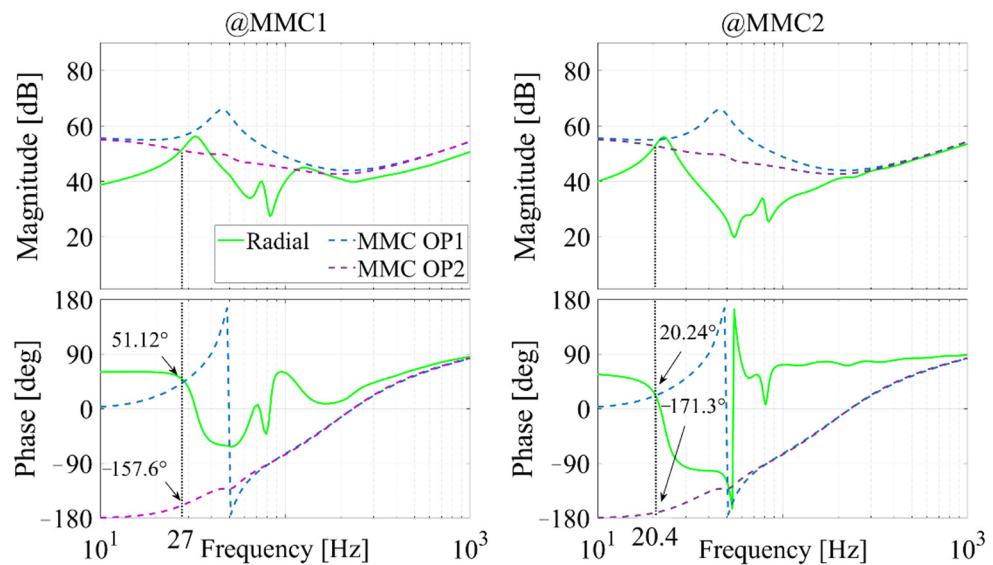
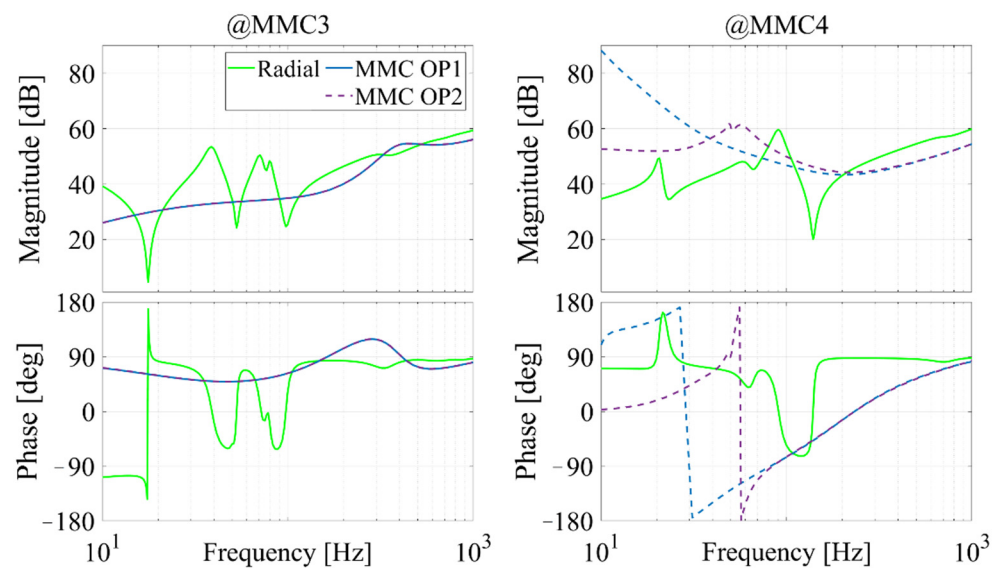
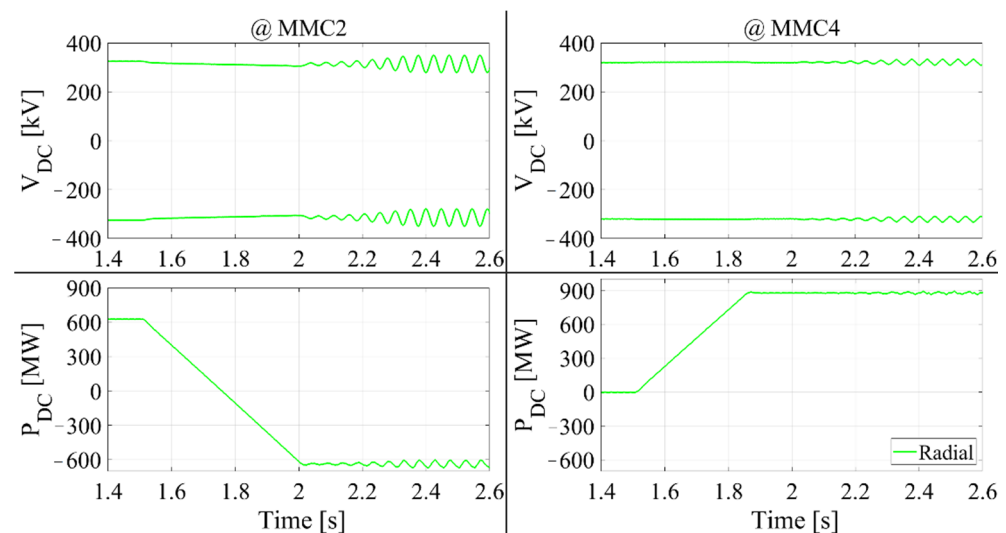


Figure 13. Impedance of MMC station 1&2 and network impedance seen from the terminals of MMC stations 1&2.

The results show a stable system for the equivalent radial network impedances seen from MMC 3 and 4 for both operating points OP1 and OP2. Stability analysis at MMC 1 and MMC 2 at OP2 results in an instability, at 27 Hz and 20.4 Hz, respectively. The obtained results are verified via a time-domain simulation in Figure 15. Here, as soon as MMC 2 reaches  $P_2 = -0.5$  p.u at  $t = 2.0$  s, oscillations with a frequency  $\sim 21$  Hz appear at the measured DC voltage and active power, which correspond to the instabilities predicted at MMC 2.



**Figure 14.** Impedance of MMC station 3&4 and network impedance seen from the terminals of MMC stations 3&4.



**Figure 15.** Time-domain verification for OP2.

## 6. Discussion

In this paper, an impedance calculation method is proposed that allows fast calculation of the DC-network impedance as seen from the DC terminals of an involved converter station. This overall DC-side network impedance, which is needed for comprehensive impedance-based stability analysis, is derived mathematically from the impedances of the grid elements. Furthermore, the proposed method is suitable for black-box converter models and therefore applicable for multi-vendor based MTDC network stability analyses. The proposed DC network impedance calculation method utilizes two widely applied approaches in relevant studies: a frequency-sweep impedance measurement approach that is suitable for black-box models in order to measure the equivalent impedances of the MMCs for different control configurations and operating points, and FD Pi-sections for emulating the frequency dependency of DC cables. Using these existing approaches, the main contribution of this paper is the proposed impedance combination of the different elements to achieve highly accurate impedances of radial MTDC networks in a very short time. As shown in the paper, the impedance is influenced by the control modes and operating points in addition to the network topology, such that a multitude of impedances that can

easily reach the range of several hundreds. These numerous impedances can be calculated by the proposed method in several minutes, whereas applying a simulative approach would require several hours for a single test case. Additional to the fast calculation, the results in the paper show that the proposed method shows a very good accuracy for radial networks and can be applied to conduct corresponding impedance-based stability analysis, thereby predicting with high accuracy possible negative converter control interactions and resulting oscillations.

In the case of meshed networks, the proposed impedance calculation methods shows limitations, as the accuracy from the results indicated that the proposed method can be used for a basic assessment of critical scenarios. Here, a verification with corresponding simulative approaches is required. Future work can focus on the enhancement of the impedance calculation method so that it can be applied to meshed networks to achieve highly accurate results.

**Author Contributions:** Conceptualization, F.L., P.D. and C.B.; methodology, F.L.; investigation, F.L.; resources, P.D., C.B.; writing—original draft preparation, F.L., P.D.; writing—review and editing, P.D., C.B., A.M.; visualization, F.L., P.D., C.B.; supervision, A.M.; All authors have read and agreed to the published version of the manuscript.

**Funding:** This research received no external funding.

**Conflicts of Interest:** Authors declare no conflict of interest.

## References

- PROMOTioN. *Deliverable 12.4: Final Deployment Plan*; Technical Report, PROMOTioN Project; PROMOTioN—Progress on Meshed HVDC Offshore Transmission Networks: Arnhem, The Netherlands, 2020.
- Rodriguez, P.; Rouzbehi, K. Multi-terminal DC grids: Challenges and prospects. *J. Mod. Power Syst. Clean Energy* **2017**, *5*, 515–523. [[CrossRef](#)]
- Nghiem, A.; Pineda, I. *Wind Energy in Europe: Scenarios for 2030*; WindEurope: Brussels, Belgium, 2017. Available online: <https://windeurope.org> (accessed on 30 June 2021).
- Hatziargyriou, N.; Milanović, J.; Rahmann, C.; Ajarapu, V.; Cañizares, C.; Erlich, I.; Hill, D.; Hiskens, I.; Kamwa, I.; Pal, B.; et al. *Stability Definitions and Characterization of Dynamic Behavior in Systems with High Penetration of Power Electronic Interfaced Technologies*; Technical Report PES-TR77; Power System Dynamic Performance Committee IEEE PES Piscataway: Piscataway, NJ, USA, 2020.
- Rault, P.; Despouys, O. *D9.3: BEST PATHS DEMO#2 Final Recommendations For Interoperability Of Multivendor HVDC Systems*; Technical Report; Best Paths: Madrid, Spain, 2018.
- Lyu, J.; Cai, X.; Molinas, M. Impedance modeling of modular multilevel converters. In Proceedings of the Impedance Modeling of Modular Multilevel Converters IECON 9-12, Yokohama, Japan, 9–12 November 2015; pp. 180–185.
- Far, A.J.; Jovicic, D. Small-Signal Dynamic DQ Model of Modular Multilevel Converter for System Studies. *IEEE Trans. Power Deliv.* **2016**, *31*, 191–199.
- Li, Z.; Wang, Z.; Wang, Y.; Yin, T.; Mei, N.; Yue, B.; Lei, W. Accurate Impedance Modeling and Control Strategy for Improving the Stability of DC System in Multiterminal MMC-Based DC Grid. *IEEE Trans. Power Electron.* **2020**, *35*, 10026–10049. [[CrossRef](#)]
- Saad, H.; Schwob, A.; Vernay, Y. Study of Resonance Issues between HVDC Link and Power System Components Using EMT Simulations. In Proceedings of the Power Systems Computation Conference (PSCC), Dublin, Ireland, 11–15 June 2018.
- Sun, J. Impedance-Based Stability Criterion for Grid-Connected Inverters. *IEEE Trans. Power Electron.* **2011**, *26*, 3075–3078. [[CrossRef](#)]
- Quester, M.; Loku, F.; Yelliseti, V.; Puffer, R. Online Impedance Measurement of a Modular Multilevel Converter. In Proceedings of the 2019 IEEE PES Innovative Smart Grid Technologies Europe (ISGT-Europe), Bucharest, Romania, 29 September–2 October 2019.
- Quester, M.; Loku, F.; Yelliseti, V.; Moser, A. Frequency Behavior of an MMC Test Bench System. In Proceedings of the 2020 6th IEEE International Energy Conference (ENERGYCon), Gammarth, Tunisia, 29 September–1 October 2020.
- D’Arco, S.; Suul, J.A.; Beerten, J. Configuration and Model Order Selection of Frequency-Dependent  $\pi$  Models for Representing DC Cables in Small-Signal Eigenvalue Analysis of HVDC Transmission Systems. *IEEE J. Emerg. Sel. Top. Power Electron.* **2021**, *9*, 2410–2426. [[CrossRef](#)]
- Beerten, J.; D’Arco, S.; Suul, J.A. Frequency-dependent cable modelling for small-signal stability analysis of VSC-HVDC systems. *IET Gener. Transm. Distrib.* **2016**, *10*, 1370–1381. [[CrossRef](#)]
- CIGRÉ Working Group B4.57. *TB 604-Guide for the Development of Models for HVDC Converters in a HVDC Grid*; CIGRE: Paris, France, 2014.
- Philipp, F.R. *HVDC Grid Protection Based on Fault Blocking Converters*; Verlagshaus Mainz GmbH Aachen: Aachen, Germany, 2020.
- CIGRÉ Working Group B4.68. *TB 811-DC Side Harmonics and Filtering in HVDC Transmission Systems*; CIGRE: Paris, France, 2020.
- Schröder, D. *Elektrische Antriebe-Regelung von Antriebssystemen*; Springer: Berlin/Heidelberg, Germany, 2015; pp. 46–87.

19. Bajracharya, C.; Molinas, M.; Suul, J.; Undeland, T. *Understanding of Tuning Techniques of Converter Controllers for VSC-HVDC*; Nordic Workshop on Power and Industrial Electronics: Espoo, Finland, 2008.
20. BEST PATHS Demo #1. *MATLAB Simulation Toolbox*; Best Paths: Madrid, Spain, 2018.
21. Quester, M.; Loku, F.; El Azzati, O.; Noris, L.; Yang, Y.; Moser, A. Investigating the Converter-Driven Stability of an Offshore HVDC System. *Energies* **2021**, *14*, 2341. [[CrossRef](#)]
22. Hahn, C. *Modellierung und Regelung selbstgeführter, höherstufiger Multiterminal-HGÜ-Systeme mit Gleichspannungszwischenkreis*; Friedrich-Alexander-Universität: Erlangen-Nürnberg, Germany, 2018.